Microscopic theory of type-1.5 superconductivity in multiband systems

Mihail Silaev[1,2,3] and Egor Babaev[1,3]

[1]*Department of Theoretical Physics, The Royal Institute of Technology, Stockholm, SE-10691 Sweden*

[2]*Institute for Physics of Microstructures RAS, 603950 Nizhny Novgorod, Russia*

[3]*Department of Physics, University of Massachusetts, Amherst, Massachusetts 01003, USA*

(Received 6 June 2011; revised manuscript received 1 August 2011; published 15 September 2011)

We report a self-consistent microscopic theory of characteristic length scales, vortex structure, and type-1.5 superconducting state in two-band systems using two-band Eilenberger formalism.

DOI: 10.1103/PhysRevB.84.094515 PACS number(s): 74.20.Fg, 73.40.Gk, 74.25.Ha

I. INTRODUCTION

The usual classification of superconductors characterizes materials by the Ginzburg-Landau (GL) parameter κ (which is the ratio of the characteristic length scale of the order parameter variation ξ and the magnetic field penetration length λ).[1] The remarkable property is that, within the GL theory of single-component superconductivity, κ determines the major features of the phase diagram of the system in magnetic field. In type-I superconductor $\kappa < 1/\sqrt{2}$ (i.e., order parameter is the slowest varying field), vortex excitations have attractive interaction and are thermodynamically unstable in applied magnetic field. Thus, in an applied field, a type-I system forms macroscopically large normal domains.[2] For $\kappa > 1/\sqrt{2}$ (type-II superconductivity), vortices are thermodynamically stable and interact repulsively yielding a new phase in strong magnetic fields: a lattice of quantized vortices.[2,3] In the Bogomolnyi limit ($\kappa = 1/\sqrt{2}$), the vortices do not interact in the Ginzburg-Landau theory. However, indeed it should be remarked that, going to a deeper microscopic level, there are always "next-to-leading-order" microscopic corrections. These corrections, although unimportant, even slightly away from this limit, provide weak nonuniversal intervortex interactions when κ is very close to $1/\sqrt{2}$ (see, e.g., Refs. 4 and 5). Apparently, a counterpart of this limit is also possible in multicomponent systems. However, in this case, the Bogomolnyi limit could appear only via quite extreme fine tuning of parameters and, therefore, is not of much physical relevance. In this paper, we are interested only in the entirely different physics of intervortex interactions and magnetic response of multicomponent systems originating from the different fundamental length scales very far from any counterparts of Bogomolnyi limit.

A question that attracted much attention recently is whether the type-I and type-II classification is sufficient for characterizing the rapidly growing family of multicomponent systems of physical interest.[6] A clear-cut example of the system where type-I and type-II dichotomy does not hold is the projected coexistent electronic and protonic (or deuteronic) superconductivity[7] in hydrogen isotopes, their mixtures and hydrogen-rich alloys at ultrahigh compression, as well as the coexisting protonic and Σ^--hyperonic superconductivity in neutron stars. These systems have U(1) × U(1) or higher symmetries and thus several fundamental length scales associated with independently conserved fields. Consequently, the system can not be characterized by a single dimensionless parameter κ. In an applied field, the only thermodynamically stable vortex solutions are "composite" vortices where both condensates have 2π phase windings. Consequently, such vortices have cores in both components.[7,8] Importantly, it also acquires a new regime[6] for which the term "type-1.5" was coined recently.[9] In that regime, like in a type-I case, the characteristic core size of one of the components is larger than the flux-carrying area. The overlap of these cores produces attractive intervortex interaction. However, in contrast to the type-I case, these vortices have repulsive interaction at short ranges.[6,10–12] This kind of nonmonotonic vortex interaction results in the appearance of the additional "semi-Meissner" phase in low magnetic fields. In that phase, vortices form clusters where because of overlaps of cores the slowest varying density component is suppressed. Moreover, these vortex clusters coexist with the domains of the two-component Meissner state.

The recent experimental works proposed that two-band[13] electronic material MgB_2 belongs to the type-1.5 case.[9,14] The principal difference with the discussed above U(1) × U(1) theory is that interband coupling breaks the symmetry down to U(1) (for a recent discussion of microscopic details see e.g., Refs. 15 and 16). Therefore, there is a single superconducting phase transition at a single T_c. However, at the same time, the system has two gaps and two superfluid densities, which, in general vary at distinct characteristic length scales at any finite distance from T_c. Therefore, the type-1.5 magnetic response can arise even infinitesimally far away from T_c from the interplay of two density modes that originate from the underlying two-gap physics. This behavior was demonstrated in the framework of phenomenological two-component U(1) GL models.[10,11]

Here, we develop a theory of type-1.5 superconductivity based on a microscopic theory without involving a GL expansion. That is, in this work, we use the Eilenberger formalism and demonstrate the existence as well as describe basic properties of type-1.5 superconductivity in multiband materials.

II. MICROSCOPIC DESCRIPTION OF VORTEX STATE IN MULTIBAND SUPERCONDUCTOR

A. Eilenberger formalism

We consider a superconductor with two overlapping bands at the Fermi level.[13] The corresponding two sheets of the Fermi surface are assumed to be cylindrical. Within quasiclassical approximation, the band parameters characterizing the two

different sheets of the Fermi surface are the Fermi velocities V_{Fj} and the partial densities of states (DOS) ν_j, labeled by the band index $j = 1,2$. We normalize the energies to the critical temperature T_c and length to $r_0 = \hbar V_{F1}/T_c$. The system of Eilenberger equations for two bands is

$$\begin{aligned} v_{Fj}\mathbf{n_p}(\nabla + i\mathbf{A})\, f_j + 2\omega_n f_j - 2\Delta_j g_j = 0, \\ v_{Fj}\mathbf{n_p}(\nabla - i\mathbf{A})\, f_j^+ - 2\omega_n f_j^+ + 2\Delta_j^* g_j = 0. \end{aligned} \tag{1}$$

Here, $\omega_n = (2n+1)\pi T$ are Matsubara frequencies and $v_{Fj} = V_{Fj}/V_{F1}$. The vector $\mathbf{n_p} = (\cos\theta_p, \sin\theta_p)$ parametrizes the position on two-dimensional (2D) cylindrical Fermi surfaces. The quasiclassical Green's functions in each band obeys normalization condition $g_j^2 + f_j f_j^+ = 1$. The self-consistency equation for the gaps is

$$\Delta_i = T\sum_{n=0}^{N_d}\int_0^{2\pi} \lambda_{ij} f_j d\theta_p. \tag{2}$$

The coupling matrix λ_{ij} satisfies the symmetry relations $n_1\lambda_{12} = n_2\lambda_{21}$, where n_i are the partial DOS normalized so that $n_1 + n_2 = 1$. We consider $\lambda_{11} > \lambda_{22}$ and therefore refer to the first band as "strong" and to the second as "weak." The vector potential satisfies the Maxwell equation

$$\nabla \times \nabla \times \mathbf{A} = \mathbf{j}, \tag{3}$$

where the current is

$$\mathbf{j} = -T\sum_{j=1,2}\sigma_j \sum_{n=0}^{N_d} Im\int_0^{2\pi} \mathbf{n_p} g_j d\theta_p. \tag{4}$$

The parameters σ_j are given by

$$\sigma_j = \pi\left(\frac{4e}{c}\right)^2 (r_0 V_{F1})^2 \nu_j v_{Fj}.$$

B. Multiple masses of the Δ fields

First, we focus on the structure of an isolated axially symmetric vortex characterized by the nontrivial phase winding of the gap functions $\Delta_{1,2} = |\Delta_{1,2}|(r)e^{i\varphi}$. We begin by finding the asymptotics of the gap function modules $|\Delta_{1,2}|(r)$ at distances far from the vortex core. In this case, the Eilenberger equations (1) can be linearized by generalizing the methods used for single-band superconductors.[17] The details of the asymptotics derivation are given in Appendix A. We rewrite Eqs. (1) in terms of the deviations from the vacuum-state values $\bar\Delta_j = \Delta_{j0} - |\Delta_j|$ and $\bar f_j = f_{j0} - f_j$, $\bar f_j^+ = f_{j0}^+ - f_j^+$ keeping on the left side the first-order terms. Then, we take the real part of Eqs. (1) to obtain the following system:

$$\begin{aligned} v_{Fj}\mathbf{n_p}\nabla \bar f^r_{\Sigma j} + 2\omega_n \bar f^r_{dj} = X^r_{\Sigma j}, \\ v_{Fj}\mathbf{n_p}\nabla \bar f^r_{dj} + 2\frac{\Omega_n^2}{\omega_n}\bar f^r_{\Sigma j} - \frac{4\omega_n}{\Omega_{nj}}\bar\Delta_j = X^r_{dj}, \end{aligned} \tag{5}$$

where $\Omega_{nj} = \sqrt{\omega_n^2 + \Delta_{0j}^2}$, $\bar f^r_{\Sigma j} = \mathrm{Re}[\bar f_j + \bar f_j^+]$, and $\bar f^r_{dj} = \mathrm{Re}[\bar f_j - \bar f_j^+]$. In Eqs. (5), the higher-order terms in $\bar\Delta_j$, $\bar f$, and $\bar f^+$ are incorporated in the right-hand-side (r.h.s) source functions $X_{\Sigma(d)j} = X_{\Sigma(d)j}(\mathbf{n_p}, \omega_n, \mathbf{r})$.

The solution of Eqs. (5) can be found in the momentum representation $f^r_{\Sigma(d)j}(\mathbf{k}) = \int f^r_{\Sigma(d)j}(\mathbf{r})\exp(-i\mathbf{kr})d^2\mathbf{r}$. After substituting it to the self-consistency equation, we get the expression for the gap functions

$$\bar\Delta_i(k) = \hat R^{-1}_{ij} N_j(k). \tag{6}$$

The elements of the matrix $\hat R = \hat R(k)$ are $R_{ii} = (\lambda_{ii}S_i - 1)$ and $R_{ij} = \lambda_{ij}S_j$, where

$$S_j(k) = 4\pi T\sum_{n=0}^{N_d}\frac{\omega_n^2}{\Omega_{nj}^2}\left[4\Omega_{nj}^2 + (v_{Fj}k)^2\right]^{-1/2}. \tag{7}$$

The source functions $N_j(k)$ come from the r.h.s of Eqs. (5). The strict definition of source functions is given in Appendix A.

The real-space asymptotic of the gap functions (6) is determined by the contributions of the singularities of the response function $\hat R^{-1}(k)$, which are poles at the zeros of the determinant $D_R(k) = \mathrm{Det}[\hat R(k)]$ and branch points at $k = 2i\Omega_{nj}/v_{Fj}$. Similarly to Ref. 17, we assume the branch cuts to lie along the imaginary axis from $k = 2i\Omega_{nj}/v_{Fj}$ to $k = i\infty$. To find the asymptotics of the gaps $\bar\Delta_i(r)$, we need only to take into account the poles of $\hat R^{-1}(k)$ lying in the upper complex half plane below all the branch cuts. In this case, all the zeros of the function $D_R(k)$ are purely imaginary $k = i\mu_n$. Each of them can be associated with the particular mass μ_n of the *composite mode* formed by a *superposition* of gap functions in two superconducting bands. The composite character of the modes arises in our case because the two bands are directly coupled. The inverse of the mass controls the characteristic length scale at which this superposition of the gap fields varies. Therefore, the lightest mass determines very-long-distance decay of *both* $\bar\Delta_1$ *and* $\bar\Delta_2$. The contribution from the branch cut contains all the length scales, which are smaller than the threshold ones given by position of the lowest branch point $k = iq_{bp}$, where $q_{bp} = 2\min(\Omega_{02}/v_{F2}, \Omega_{01}/v_{F1})$.

Equation (6) results in the asymptotical expression for the gap functions

$$\bar\Delta_i(r) = \int_0^r dr_1 G_{ij}(r,r_1)N_j(r_1).$$

Here, $N_j(r)$ is the Fourier-Bessel image of the source function in Eq. (6) and

$$\begin{aligned} \hat G(r,r_1) = \sum_n \hat A_n K_0(q_n r) I_0(q_n r_1) \\ + \frac{2}{\pi}\int_{q_{bp}}^{\infty} ds\, s K_0(sr) I_0(sr_1)[\hat R^{-1}]_{k=is}, \end{aligned} \tag{8}$$

where K_0 and I_0 are MacDonald and modified Bessel functions. The matrices $\hat A_n$ determining the contributions of the pole terms are

$$\hat A_n = 2ik\left[\frac{dD_R}{dk}\right]^{-1}\begin{pmatrix} R_{22} & -R_{12} \\ -R_{21} & R_{11}\end{pmatrix}|_{k=iq_n}, \tag{9}$$

and the branch-cut contribution is determined by the the jump of the response function

$$[\hat R^{-1}]_{k=is} = \hat R^{-1}(k = is + 0) - \hat R^{-1}(k = is - 0). \tag{10}$$

Under rather general conditions, the response function in Eq. (6) has two poles given by zeros of the determinant

$D_R(k) = 0$, which lie below the branch cuts. Thus, in this case the asymptotical behavior of the gap functions is principally different from the single-band superconductor, despite the fact that they share the same U(1) symmetry of the order parameter. The two poles determine the *two inverse length scales* or, equivalently, the two masses of composite gap functions fields, which we denote as "heavy" $1/\xi_H = \mu_H$ and "light" $1/\xi_L = \mu_L$ (i.e., $\mu_H > \mu_L$). The corresponding composite gap function modes are parametrized by the two "mixing angles" θ_L,θ_H as follows:

$$\begin{pmatrix} \tilde{\Delta}_L \\ \tilde{\Delta}_H \end{pmatrix} = \begin{pmatrix} \cos\theta_L & \sin\theta_L \\ -\sin\theta_H & \cos\theta_H \end{pmatrix} \begin{pmatrix} \bar{\Delta}_1 \\ \bar{\Delta}_2 \end{pmatrix}. \qquad (11)$$

Note that, in the two-band GL theory without interband impurity scattering terms, one has $\theta_L = \theta_H$.[10,11] Below, we recover this behavior at elevated temperatures without using GL-type expansion, thereby verifying predictions of phenomenological GL models. However, outside the range of validity of the GL theory, we find that $\theta_L \neq \theta_H$.

Let us now consider in detail an example of the system with $\lambda_{11} = 0.25, \lambda_{22} = 0.213, n_1 = n_2 = 0.5$, and various values of the interband coupling $\lambda_J = \lambda_{12} = \lambda_{21}$. We focus on the two different regimes, determined by the band parameter $\gamma_F = v_{F2}/v_{F1}$, namely, (i) $\gamma_F > 1$ and (ii) $\gamma_F < 1$.

(i) Some of the basic properties of this regime are captured by the particular case when $\gamma_F = 1$. The examples of the temperature dependencies of the masses $\mu_{L,H}(T)$ are shown in Fig. 1(a). The two massive modes coexist at the temperature interval $T_1^* < T < T_c$, where the temperature T_1^* is determined by the branch-cut position, shown in Fig. 1(a) by black dashed line. For temperatures $T < T_1^*$, there exists only one massive mode. At very low temperatures, the mass μ_L is very close to the branch cut. As the interband coupling parameter is increased, the temperature T_1^* rises and becomes equal to T_c at some critical value of $\lambda_J = \lambda_{Jc}$. For the particular case of $\gamma_F = 1$, we found an exact condition $\lambda_{Jc} = \lambda_{22}$. The evolution of the masses $\mu_{L,H}$ is shown in the sequence of plots in Figs. 2(a)–2(d) for λ_J increasing from the small values $\lambda_J \ll \lambda_{11},\lambda_{22}$ to the values comparable to intraband coupling $\lambda_J \sim \lambda_{11},\lambda_{22}$.

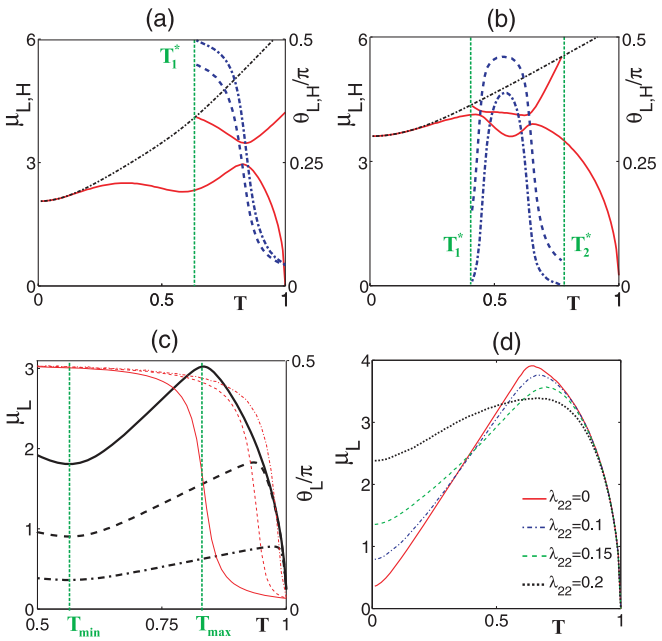

FIG. 1. (Color online) Masses $\mu_{L,H}$ of the composite gap function fields for (a) $\gamma_F = 1$ and $\lambda_J = 0.005$, (b) $\gamma_F = 0.5$ and $\lambda_J = 0.0025$. The position of branch cut is shown by black dashed line. The mixing angles $\theta_{L,H}$ are shown by blue dashed and dashed-dotted lines correspondingly. (c) Temperature dependence of the mass $\mu_L(T)$ (black thick curves) and the corresponding mixing angle θ_L determined by Eq. (11) (red thin curves) for $\gamma_F = 1$, 2, 5 (solid, dashed, and dashed-dotted curves). The coupling parameters are $\lambda_{11} = 0.25$, $\lambda_{22} = 0.213$, and $\lambda_J = 0.005$. (d) Temperature dependence of the mass $\mu_L(T)$ for different values of coupling constant λ_{22}.

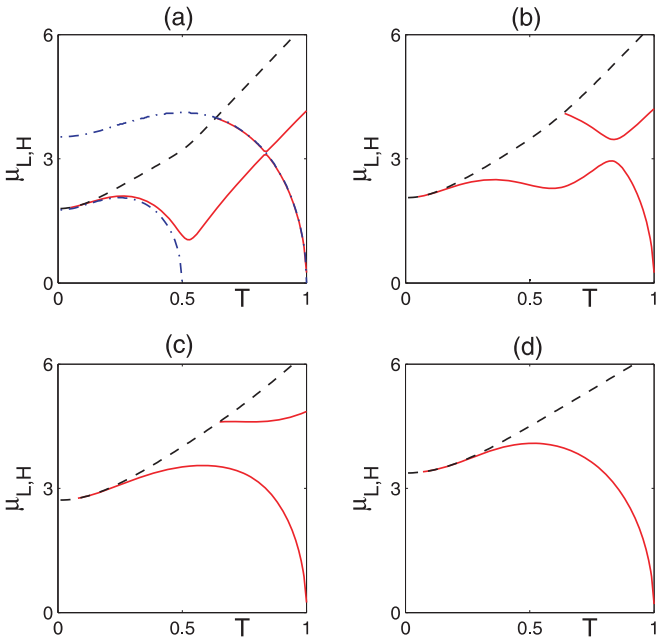

FIG. 2. (Color online) Masses μ_L and μ_H (red solid lines) of the composite gap function fields for the different values of interband Josephson coupling λ_J and $\gamma_F = 1$. In the sequence of plots (a)–(d), the transformation of masses is shown for λ_J increasing from the small values $\lambda_J \ll \lambda_{11},\lambda_{22}$ to the values comparable to intraband coupling $\lambda_J \sim \lambda_{11},\lambda_{22}$. The particular values of coupling constants are $\lambda_{11} = 0.25$, $\lambda_{22} = 0.213$, and $\lambda_J = 0.0005$, 0.0025, 0.025; λ_{22} for plots (a)–(d) correspondingly. The branch cuts are shown by black dashed lines. In (a), with blue dashed-dotted lines, the masses of modes are shown for the case of $\lambda_J = 0$. Note that, at $\lambda_J = 0$, the two masses go to zero at two different temperatures. Because $1/\mu_{L,H}$ are related to the coherence lengths, this reflects the fact that, for U(1) × U(1) theory, there are two independently diverging coherence lengths. Note that, for finite values of interband coupling, only one mass μ_L goes to zero at one T_c.

(ii) In the case if $\gamma_F < \gamma_{th}$ (where γ_{th} is a characteristic value determined by the system parameters), the two massive modes coexist at some temperature interval $T_2^* < T < T_1^*$ where $T_1^* \leqslant T_c$. For the particular case when $\gamma_F = 0.5$, the temperature dependencies of $\mu_{L,H}(T)$ are shown in Fig. 1(b).

In Figs. 1(a) and 1(b), the mixing angles θ_L and θ_H given by Eq. (11) are shown by blue dashed and dashed-dotted lines, correspondingly. In the case (i) near the critical temperature, the angles are approximately equal, which provides for this regime a microscopic verification for of the results obtained

using phenomenological GL theories.[10,11] At lower temperatures, the discrepancy is considerable and grows with the increasing interband coupling.

Large deviations of the mixing angle from 0 and $\pi/2$ signal strong mixing of the gap fields. It occurs near the avoided crossing points of $\mu_L(T)$ and $\mu_H(T)$. In case (i) shown in Fig. 1(a), there is one avoided crossing point and in the case (ii), there can be two of them, as shown in Fig. 1(b).

The above-discussed existence of two modes associated with mixed gap functions can, under certain conditions, result in the type-1.5 behavior as it was demonstrated in the framework of GL approach.[10,11] However, importantly, the microscopic formalism we use here allows us to describe type-1.5 superconductivity beyond the validity of GL models. The type-1.5 behavior requires a density mode with low mass μ_L to mediate intervortex attraction at large separations, which should coexist with short-range repulsion.

We find that the temperature dependence of $\mu_L(T)$ is characterized by an anomalous behavior, which is in strong contrast to temperature dependence of the mass of the gap mode in single-band theories. As shown on Fig. 1(c), the function $\mu_L(T)$ is *nonmonotonic* with the minimum at the temperature $T_{\min}$. The minimum is close to the crossover temperature where the second superconducting band becomes active. The maximum is located at the temperature $T_{\min} < T_{\max} < T_c$.

The structure of the composite gap function mode [shown in Fig. 1(c)] $\tilde{\Delta}_L$ is characterized by the mixing angle θ_L given by Eq. (11). At the temperature interval $T < T_{\max}$, the mixing angle is $\theta_L \approx \pi/2$. Therefore, in this temperature regime, the mode with lightest mass consists primarily of the weak band gap $\bar{\Delta}_2(r)$ with a tiny admixture of $\bar{\Delta}_1(r)$. Note that, in this regime, the overall behavior of $|\Delta_1|(r)$ outside the long-range asymptotic tail has relatively weak dependence on interband coupling (i.e., at larger distances from the core it has slowly recovering tail associated with only tiny suppression relative to its ground-state value). At the same time, the recovery of $|\Delta_2|(r)$ to a larger degree is dominated by the light mass mode.

C. High-temperature limit

As noted above at elevated temperatures, the mixing angles have close values, consistent with the type-1.5 behavior, which appear in the framework of two-band Ginzburg-Landau models.[11] At very high temperatures $T_{\max} \ll T < T_c$, the mixing angle θ_L gradually becomes small $\theta_L \ll \pi$, which means that there the mode $\tilde{\Delta}_L$ is dominated by the strong band contribution $\bar{\Delta}_1$.

Since any Josephson interband coupling breaks the symmetry of the system in question down to U(1), then according to Ginzburg-Landau argument, this symmetry dictates that, asymptotically, *in the limit* $T \to T_c$, one should recover a single-component-like GL temperature dependence $\mu_L \sim \sqrt{1 - T/T_c}$ of a single order parameter (at the level of mean-field theory).[1]

In the regimes corresponding to Figs. 1(a) and 1(c) very close to T_c, the mixing angle of the heavy mode is small $\theta_H \ll 1$, which makes the contribution of the smaller gap $\bar{\Delta}_2$ to the heavy mode the dominating one. This behavior of the mixing angles, and the fact that for nonzero Josephson coupling only one mass $\mu_L(T)$ goes to zero at $T \to T_c$, allows one to neglect the heavy mode and construct a mean-field GL order parameter with the scaling $\mu_L \sim \sqrt{1 - T/T_c}$ *as an "asymptotic" characteristic* in the limit $T \to T_c$. However, as shown in Fig. 1(c), the temperature region of such behavior shrinks drastically for large disparities of the band characteristics and weak interband couplings. In general, the smaller the interband coupling, the closer to T_c one should be in order to obtain single-component-like GL scaling. For a wide range of parameters, the mean-field GL theory with the single-component-like GL scaling $\mu_L \sim \sqrt{1 - T/T_c}$ will emerge only infinitesimally close to T_c. Note that the limit where $\mu_L \sim \sqrt{1 - T/T_c}$ is in certain cases unphysical because the underlying mean-field theory can become invalid because of fluctuations, at temperatures lower that the temperature where this scaling would take place. Thus, even in weak-coupling two-band systems with U(1) symmetry for a wide parameter range, one could not apply a leading order in $(1 - T/T_c)$ GL theory since the region of its applicability will fall into the parameter space where underlying mean-field theory is not valid because of fluctuations. In contrast to single-component systems, as a consequence of the presence of two gaps even slightly away from T_c, the behavior of $\mu_L(T)$ can be drastically different from the usual GL scaling. As a result, the product $\Lambda\mu_L$ where Λ is the magnetic field penetration length acquires a strong temperature dependence. Moreover, as we show below, its limiting value at T_c does not determine entirely the intervortex interaction potential nor the magnetic response of the system. Therefore, one can not in general parametrize the magnetic response of two-band systems by the single GL parameter $\kappa = \Lambda/\xi$.

D. Light mode of gap function field and type-1.5 behavior

The plots of $\mu_L(T)$ for $\gamma_F = 1, 2, 5$ are shown in Fig. 1(c) by solid, dashed, and dashed-dotted thick black lines. There is a clear general tendency of increasing $T_{\max}$ with growing parameter γ_F, which characterizes band disparity. It leads to broadening of the temperature region of the anomalous behavior of the mass $\mu_L(T)$ where the field's asymptotics are dominated by the weak band. Figure 1(c) clearly demonstrates the considerable overall suppression of μ_L with growing parameter γ_F. The inverse of the mass of the light composite gap mode μ_L sets the range of the attractive density-density contribution to intervortex interaction. Therefore, the condition for the occurrence of the intervortex attraction will be met if μ_L is smaller than Λ^{-1}.

Thus, a physically important situation arising in a two-band superconductor is that, for a wide range of parameters even slightly away from T_c, the temperature dependence of μ_L is dramatically different from that of the inverse magnetic field penetration length Λ^{-1}.

Furthermore, because the softest mode with the mass μ_L in the two-band system may be associated with only a fraction of the total condensate, and because there could be the second mixed gap mode which can have larger mass μ_H, the short-range intervortex interaction can be repulsive. Since ultimately the sign of the long-range interaction is decided by the competition of Λ^{-1} and μ_L, we plot their temperature dependencies in Fig. 3(a). It shows how in these cases the

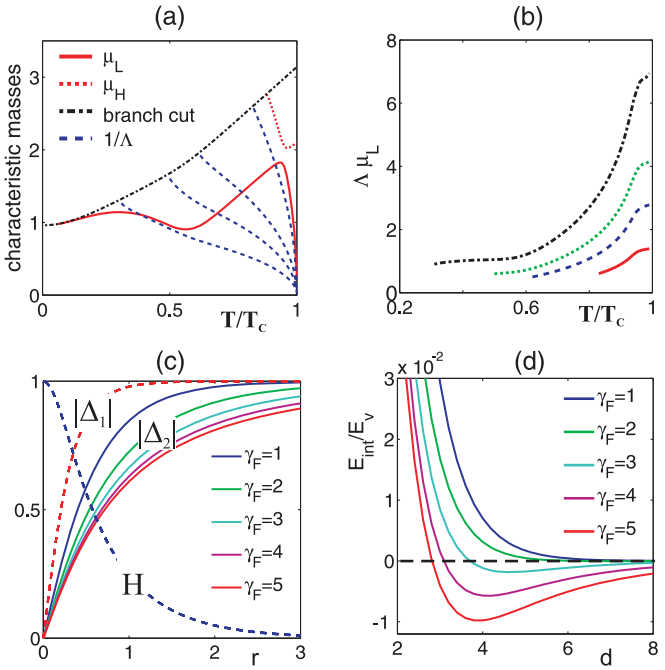

FIG. 3. (Color online) (a) Masses μ_L and μ_H (red solid and dotted lines) of the composite gap function fields and inverse London penetration (blue dashed lines) for the different values of $\Lambda\mu_L(T_c)/\sqrt{2}$ =1, 2, 3, 5. The position of branch cut is shown by black dashed-dotted line. (b) The temperature dependence of the quantity $\Lambda\mu_L$ for $\Lambda\mu_L(T_c)/\sqrt{2}$ =1, 2, 3, 5 (red solid, blue dashed, and black dashed-dotted lines). (c) Distributions of magnetic field $H(r)/H(r=0)$, gap functions $|\Delta_1|(r)/\Delta_{10}$ (dashed lines), and $|\Delta_2|(r)/\Delta_{20}$ (solid lines) in a single vortex for the coupling parameters $\lambda_{11}=0.25$, $\lambda_{22}=0.213$, and $\lambda_{21}=0.0025$ and different values of the band parameter γ_F =1, 2, 3, 4, 5. (d) The energy of interaction between two vortices normalized to the single vortex energy as function of the intervortex distance d. In panels (c) and (d) the temperature is $T=0.6$.

system goes from type-II to type-1.5 behavior as temperature is decreased. The type-1.5 behavior sets in when μ_L becomes smaller than Λ^{-1}, and the density associated with the light mode is small enough that the system has a short-range intervortex repulsion.

To contrast the physics of fundamental modes in the two-band case with the single-band case, we plot on Fig. 3(b) the product of Λ and μ_L. Note that only *infinitesimally* close to T_c can this product can be interpreted as GL paramter κ because the inverse mass $\sqrt{2}\mu_L^{-1}$ becomes the single-component-like GL coherence length. However, away from T_c, it represents a mass of the softest of competing modes and the product $\Lambda\mu_L$ has a strong and nonmonotonic temperature dependence shown on Fig. 3(b).

III. SELF-CONSISTENT CALCULATION OF THE VORTEX STRUCTURE AND NONMONOTONIC VORTEX INTERACTION ENERGY

Next, we calculate self-consistently the structure of isolated vortex for different values of γ_F. In these calculations, we fix the values of parameters σ_i by adjusting the partial DOS, which in the case of cylindrical Fermi surfaces is regulated by the ratio of effective masses so that $n_2=n_1/\gamma_F$ and $\lambda_{12}=\lambda_{21}/\gamma_F$. We chose the following values of the coupling parameters $\lambda_{11}=0.25, \lambda_{22}=0.213$. The interband interaction is small $\lambda_{21}=0.0025$ and the temperature is $T=0.6$ when $\Delta_{10}\gg\Delta_{20}$. In this case, the composite gap function mode $\tilde{\Delta}_L(r)$ consists mainly of the weak gap $\bar{\Delta}_2(r)$. Thus, although at the very long ranges the behavior of both $|\Delta_1|(r)$ and $|\Delta_2|(r)$ are determined by the same mass μ_L, the overall behavior (i.e., outside asymptotic regimes) of the gap $|\Delta_1|(r)$ [shown by red dashed lines in Fig. 3(c)] is not very sensitive to the parameter γ_F. A complex aspect of the vortex structure in the two-band system is that, in general, the exponential law of the asymptotic behavior of the gaps is *not* directly related to the "core size" at which gaps recover most of their ground-state values. We can characterize this effect by defining a "healing" length $L_{\Delta i}$ of the gap function as follows: $|\Delta_i|(L_{\Delta i})=0.95\Delta_{i0}$. Then, we obtain that $L_{\Delta 1}\approx 0.8$ for all values of γ_F. On the contrary, the healing length $L_{\Delta 2}$ changes significantly such that $L_{\Delta 2}=1.6, 2.5, 3.2, 3.9, 4.5$ for $\gamma_F=1, 2, 3, 4, 5$, correspondingly.

To demonstrate the type-1.5 behavior, we have chosen the parameters σ_i in the self-consistency equation for the current such that the characteristic magnetic field localization length $L_H\approx 2$ is much larger than $L_{\Delta 1}$. This leads to an existence of regular vortex lattices in a wide range of strong magnetic fields (i.e., when vortices are closely packed and thus experience only strong short-range repulsive interaction). However, the high magnetic field behavior notwithstanding, the vortex structures shown in Fig. 3(c) clearly show that $L_{\Delta 1}\ll L_H\ll L_{\Delta 2}$, i.e., the long-range interaction is attractive and, thus, the system in fact belongs to the type-1.5 regime.

Next, to demonstrate the type-1.5 superconductivity, i.e., large-scale attraction and small-scale repulsion of vortices, which originate from disparity of the variations of two gaps, we explicitly calculate the intervortex interaction energy. We evaluate the two-band generalization of the Eilenberger expression for the free energy of the two vortices positioned at the points $\mathbf{r_R}=(d/2,0)$ and $\mathbf{r_L}=(-d/2,0)$ in the xy plane. Here, we generalize to two-band theory the method developed for calculation of asymptotic vortex interaction in single-component theories.[18] The method assumes that, for large separations, in the region $x<0$, the fields $\mathbf{H}$, $\Delta_{1,2}$, and $f_{1,2}^{(+)}$ correspond to the single vortex placed at the point $\mathbf{r_L}$ weakly perturbed by the presence of the second vortex. The interaction energy can be expressed through the integral over the line $x=0$ passing in the middle between vortices $E_{\rm int}=2\int_{-\infty}^{\infty}dy\,\tilde{E}_{\rm int}(y)$ where

$$\tilde{E}_{\rm int}=\int_{-\infty}^{\infty}dy\,H_v Q_v+T\sum_{j=1,2}\sum_{\omega_n>0}\frac{\sigma_j\Delta_{0j}}{4\omega_n}\times\int_0^{2\pi}d\theta_p\cos\theta_p(f_{Lj}f_{Rj}^{+}-f_{Lj}^{+}f_{Rj}). \quad (12)$$

The detailed derivation of the above expression can be found in Appendix B. The indices $R(L)$ correspond to the solutions of Eilenberger equations (1) for isolated vortices positioned at the points $\mathbf{r_{R(L)}}$. The first term in Eq. (12) contains the magnetic field $H_v(|\mathbf{r}-\mathbf{r_L}|)$ and the axial component of

superfluid velocity distribution $Q_v(|\mathbf{r}-\mathbf{r_L}|)$ corresponding to the isolated vortex placed at the point $\mathbf{r}=\mathbf{r_L}$.

In Fig. 3(d), the interaction energy $E_{\rm int}$ is shown as a function of the distance between two vortices d. The energy $E_{\rm int}$ is normalized to the single vortex energy E_v. The plots on Fig. 3(d) clearly demonstrate the emergence of type-1.5 behavior when the parameter γ_F is increased. This is manifested in the appearance of nonmonotonic behavior of $E_{\rm int}(d)$.

IV. LOW-TEMPERATURE VORTEX ASYMPTOTICS AND INTRINSIC PROXIMITY EFFECT

Finally, we discuss the two-band superconductor with $\Delta_{20} \ll \Delta_{10}$ at $T \to 0$. Note that a qualitatively similar regime is realized in the two-band superconductor MgB_2.[15] To model such a situation, we choose the coupling constants $\lambda_{11}=0.25$, $\lambda_{12}=\lambda_{21}=\lambda_J=0.05$, and consider various values of λ_{22}. The temperature dependencies of the mass $\mu_L(T)$ for different values of λ_{22} are shown in Fig. 1(d). Note that, in this case, decreasing of intraband coupling λ_{22} leads to the decreasing of the μ_L at low temperatures. This anomalous behavior of the characteristic length scale is clearly manifested in the vortex structure shown in Fig. 4. The near-core gap-function profiles [Figs. 4(a) and 4(c)] feature shrinkage of the vortex core at decreasing temperature, similarly to clean single-band superconductors.[19] However, the asymptotics of gap functions [Figs. 4(b) and 4(d)] are drastically different from the single-band case. Indeed, it can be seen that, in a certain temperature domain, the lower the temperature, the slower the recovery of the gap functions at large distances from the core. Such behavior in the two-band system is clearly in a sharp contrast with the overall vortex core shrinking with decreasing temperature in clean single-band superconductors.

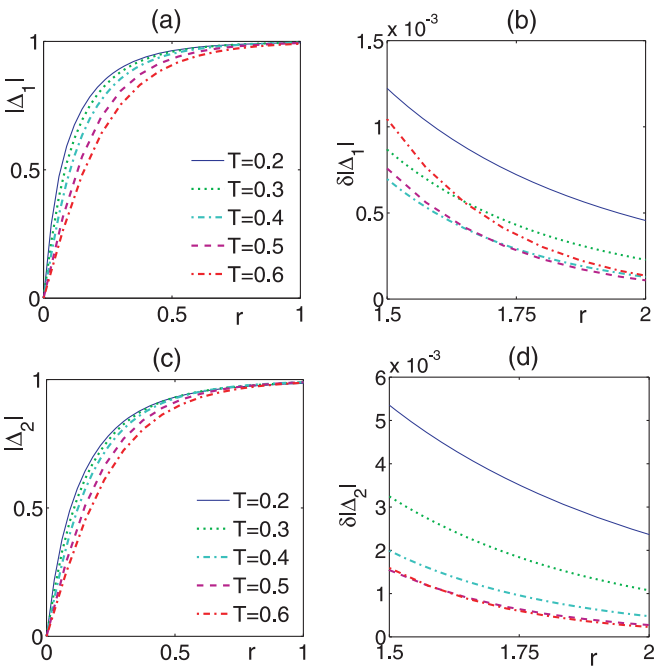

FIG. 4. (Color online) Gap-function profiles around vortex core for $\lambda_{11}=0.25$, $\lambda_{22}=0.1$, $\lambda_{12}=\lambda_{21}=0.05$. (a) and (c): Variation of the gap functions $|\Delta_j|(r)/\Delta_{j0}$ ($j=1,2$) near the core. (b) and (d): The behavior of gap-function deviations from the vacuum state $\delta\Delta_j(r)=1-|\Delta_j|(r)/\Delta_{j0}$ at longer range. Note that, in this temperature span, the *higher* the temperature, the *faster* the long distance decay of $\delta\Delta_j(r)$, which reflects the found fact in the two-band system that the field mass can increase with raising temperature [see also Fig. 1(d).]

Note that, in the above case, at low temperatures we have $\mu_L \approx 2\sqrt{\Delta_{20}^2+(\pi T)^2}/v_{F2}$. For the especially interesting regime of purely interband proximity effect-induced superconductivity in the weak band, we can consider the limit $T \gg \Delta_{20}/\pi$. Then, $\mu_L \approx \xi_N^{-1}$, where $\xi_N = v_{F2}/(2\pi T)$ is the coherence length in a pure normal metal[2] describing the penetration length of superconducting correlations induced by the proximity effect in superconductor (normal) metal (SN) hybrid structures.[20] Thus, we obtain that the intrinsic proximity effect due to the interband coupling[11] can in certain cases be described by the similar length scale as the usual one in SN hybrid structures. At the temperature interval $\Delta_{20} \ll \pi T \ll \Delta_{10}$, the mass $\mu_L(T)$ grows linearly with temperature [Fig. 1(d)].

V. CONCLUSION

In conclusion, the rapidly growing family of discovered multiband superconductors (MgB_2, iron pnictides, etc.) requires understanding and classification of possible magnetic response of systems with multiple superconducting gaps. Here, we reported a microscopic theory of magnetic response of a superconductor with two bands (the developed approach can be generalized to the case of a higher number of bands). We have shown that new physics that arises in multiband systems is the existence of several *mixed* gap modes. This, in a range of parameters, results in the existence of the type-1.5 superconducting regime.

We described the system properties and emergence of type-1.5 regimes in the entire temperature regimes, in particular, beyond the validity of a two-component GL theory. The universal feature of all the regimes supporting type-1.5 behavior is the thermodynamic stability of vortex excitations in spite of the existence of a mode, which varies at a fundamental length scale larger than the magnetic field penetration length. It results in nonmonotonic vortex interaction and appearance of the additional semi-Meissner phase in low magnetic fields, which is a macroscopic phase separation into (i) domains of two-component vortex state and (ii) vortex clusters where one of the components is suppressed.

ACKNOWLEDGMENT

The work was supported by the NSF CAREER Award No. DMR-0955902, the Knut and Alice Wallenberg Foundation through the Royal Swedish Academy of Sciences, and by the Swedish Research Council, "Dynasty" Foundation, Presidential RSS Council (Grant No. MK-4211.2011.2), and Russian Foundation for Basic Research.

APPENDIX A: ASYMPTOTICAL BEHAVIOR OF THE GAP FUNCTIONS

We focus on the structure of the isolated axially symmetric vortex in two-band superconductor characterized by the nontrivial phase winding of the gap functions

$$\Delta_{1,2} = |\Delta_{1,2}|(r)e^{i\varphi}. \tag{A1}$$

We begin by considering the asymptotical behavior of the gap functions at distances far from the vortex core when the deviations of all fields from the homogeneous values are small. In this case, the Eilenderger equations (1) can be linearized in order to find the asymptotical behavior of the gap-function modules $|\Delta_{1,2}|(r)$. To compare with the different linearization problem in the single-band case, see Ref. 21.

To determine the asymptotic behavior, we use the transformation $f \to fe^{i\varphi}$, $f^+ \to f^+e^{-i\varphi}$ and rewrite the Eilenberger equations (1) in terms of the deviations from the vacuum-state values $\bar{\Delta}_j = \Delta_{j0} - |\Delta_j|$ and $\bar{f}_j = f_{j0} - f_j$, $\bar{f}_j^+ = f_{j0}^+ - f_j^+$. Then, by keeping the first-order terms $\bar{f}_{\Sigma(d)}$ and $\bar{\Delta}_j$ in the left-hand side, we can rewrite the Eilenberger equations in the following form (we omit the band index for brevity):

$$\begin{aligned} v_F\mathbf{n}\nabla\bar{f}_\Sigma + 2\omega_n\bar{f}_d &= X_\Sigma, \\ v_F\mathbf{n}\nabla\bar{f}_d + 2\frac{\Omega_n^2}{\omega_n}\bar{f}_\Sigma - i\frac{2\Delta_0}{\Omega_n}\mathbf{nQ} - \frac{4\omega_n}{\Omega_n}\bar{\Delta} &= X_d, \end{aligned} \tag{A2}$$

where the higher-order terms in $\bar{\Delta}_j$, $\bar{f}$, and $\bar{f}^+$ are incorporated in the r.h.s. functions $X_{\Sigma(d)} = X_{\Sigma(d)}(\mathbf{n_p},\omega_n,\mathbf{r})$. In Eq. (A2), we introduce $\Omega_n = \sqrt{\omega_n^2 + \Delta_0^2}$ and the functions $\bar{f}_\Sigma = \bar{f} + \bar{f}^+$ and $\bar{f}_d = \bar{f} - \bar{f}^+$. The higher-order terms are incorporated in the functions $X_{\Sigma(d)} = X_{\Sigma(d)}(\mathbf{n_p},\omega_n,\mathbf{r})$.

Then, we take the real part of Eq. (A2) to obtain the following system:

$$\begin{aligned} v_F\mathbf{n_p}\nabla f_\Sigma^r + 2\omega_n f_d^r &= X_\Sigma^r, \\ v_F\mathbf{n_p}\nabla f_d^r + 2\frac{\Omega_n^2}{\omega_n}f_\Sigma^r - \frac{4\omega_n}{\Omega_n}\bar{\Delta} &= X_d^r. \end{aligned} \tag{A3}$$

Here, we omit the band index for brevity and denote $f_{\Sigma(d)}^r = Re\,\bar{f}_{\Sigma(d)}$. Below we will find the asymptotic of the gap fields treating the nonlinear terms in the r.h.s. of Eq. (A3) as source functions.

The solution of Eq. (A3) can be found in the momentum representation $f_{\Sigma,d}^r(\mathbf{k}) = \int f_{\Sigma,d}^r(\mathbf{r})\mathrm{e}^{-i\mathbf{kr}}d^2\mathbf{r}$. Then, we get

$$f_\Sigma^r = \frac{\omega_n^2}{\Omega_n}\frac{8\bar{\Delta}}{4\Omega_n^2 + (\mathbf{v_F}\mathbf{k})^2} + M(\mathbf{v_F}\mathbf{k},\omega_n), \tag{A4}$$

where the last term incorporates the higher-order corrections

$$M(\mathbf{v_F}\mathbf{k},\omega_n) = \frac{2\omega_n}{4\Omega_n^2 + (\mathbf{v_F}\mathbf{k})^2}\left(X_d^r - \frac{i\mathbf{v_F}\mathbf{k}}{2\omega_n}X_\Sigma^r\right). \tag{A5}$$

After substituting it to the self-consistency Eq. (2), we get the expression for the order parameter

$$\bar{\Delta}_i(k) = \hat{R}_{ij}^{-1}N_j(k), \tag{A6}$$

where

$$N_i(k) = \frac{\lambda_{ij}T}{2}\sum_{n=0}^{N_d}\int_0^{2\pi} M_j d\theta_p \tag{A7}$$

and the elements of the matrix $\hat{R} = \hat{R}(k)$ are defined by $R_{ii} = (\lambda_{ii}S_i - 1)$ and $R_{ij} = \lambda_{ij}S_j$, where

$$S_j = 4T\sum_{n=0}^{N_d}\frac{\omega_n^2}{\Omega_{nj}}\int_0^{2\pi}\frac{d\theta_p}{4\Omega_{nj}^2 + (\mathbf{v_{Fj}}\mathbf{k})^2}. \tag{A8}$$

The integrals entering the expressions (A8) above are

$$\int_0^{2\pi}\frac{d\theta_p}{b^2 + (\sin\theta_p)^2} = \frac{2\pi}{b\sqrt{b^2+1}}$$

so that

$$S_j(k) = 4\pi T\sum_{n=0}^{N_d}\frac{\omega_n^2}{\Omega_{nj}^2}\frac{1}{\sqrt{4\Omega_{nj}^2 + (v_{Fj}k)^2}}. \tag{A9}$$

The source functions $N_j(k)$ come from the nonlinear terms $X_{\Sigma,d}^r$ in Eilenberger Eq. (A3).

Equation (A6) is the two-band response function. To compare with the single-band response function, see Ref. 17. In general, the real-space asymptotic behavior of the order parameter (A6) is determined by the contributions of the singularities of the response function $\hat{R}^{-1}(k)$, which are poles and branch points at $k = 2i\Omega_{nj}/v_{Fj}$. Analogously to the consideration in Ref. 17, we assume the branch cuts to lie along the imaginary axis from $k = 2i\Omega_{nj}/v_{Fj}$ to $k = i\infty$. The poles are determined by the zeros of the determinant $D_R(k) = \mathrm{Det}\hat{R}(k) = 0$, so that

$$D_R(k) = (1 - \lambda_{11}S_1)(1 - \lambda_{22}S_2) - \lambda_{12}\lambda_{21}S_1S_2.$$

Since we are interested in the asymptotic behavior of the order parameter, we need only to take into account the poles of $\hat{R}^{-1}(k)$ lying in the upper complex half plane below all the branch cuts. In this case, all the zeros of the function $D_R(k)$ are purely imaginary $k^* = iq_n$. Each of them can be associated with the particular mass of the gap function field $\mu_n = 1/q_n$, which determines the characteristic length scale of the gap-function variation. On the other hand, the contribution from the branch cut contains all the length scales, which are larger than the threshold one given by position of the lowest branch point $k = iq_{bp}$, where

$$q_{bp} = 2\min(\Omega_{02}/v_{F2}, \Omega_{01}/v_{F1}). \tag{A10}$$

APPENDIX B: ENERGY OF INTERACTION BETWEEN TWO VORTICES

1. General free-energy expression

The two-band generalization of the Eilenberger expression for the free energy[22] reads as

$$\begin{aligned} F(\mathbf{r}) = \frac{\mathbf{H^2}}{2} &+ \tilde{\rho}_{11}|\Delta_1|^2 + \tilde{\rho}_{22}|\Delta_2|^2 \\ &+ \tilde{\rho}_J(\Delta_1\Delta_2^* + \Delta_2\Delta_1^*) + F_{I1} + F_{I2}, \end{aligned} \tag{B1}$$

where

$$\begin{pmatrix} \tilde{\rho}_{11} & \tilde{\rho}_{12} \\ \tilde{\rho}_{21} & \tilde{\rho}_{22} \end{pmatrix} = \frac{1}{\kappa^2} \begin{pmatrix} \rho_{11} & \rho_{12} \\ \rho_{21} & \rho_{22} \end{pmatrix}^{-1},$$

$\tilde{\rho}_J = \tilde{\rho}_{12} = \tilde{\rho}_{21}$, and

$$F_{Ij} = -\frac{T}{\kappa^2} \sum_{\omega_n>0} \int_0^{2\pi} n_j I_j(\omega_n,\theta_p,\mathbf{r}) d\theta_p$$

with

$$I_j(\omega_n,\theta_p,\mathbf{r}) = \Delta_j^* f_j + \Delta_j f_j^+ + (g_j - 1) \times \left[2\tilde{\omega}_n + \frac{v_{Fj}}{2} \mathbf{n_p} \nabla (\ln f_j - \ln f_j^+) \right], \quad \text{(B2)}$$

where $j = 1,2$ and

$$\tilde{\omega}_n = \omega_n + i v_{Fj} \mathbf{n_p} \mathbf{A}/2.$$

Then, the variation of the free energy (B1) with respect to the fields $\mathbf{A}$ and Δ gives the self-consistency equations (4) and (2), correspondingly. The variation over f and f^+ with the normalization condition taken into account yields the Eilenberger equations (1). Provided the functions f, f^+, g satisfy Eqs. (1), the expression (B2) can be rewritten as

$$I_j(\omega_n,\theta_p,\mathbf{r}) = \frac{\Delta_j^* f_j + \Delta_j f_j^+}{1 + g_j}. \quad \text{(B3)}$$

2. Linearized theory of vortex interaction

To calculate the energy of vortex interaction, we evaluate the free-energy expression for the system of two vortices positioned at the points $\mathbf{r_R} = (d/2,0)$ and $\mathbf{r_L} = (-d/2,0)$ in the xy plane. Here, we employ the method similar to that in Ref. 18.

Let us consider the half-plane $x < 0$ containing only one of the vortices. We decompose the gap function into amplitude and phase (we omit the band index for brevity)

$$\Delta(\mathbf{r}) = |\Delta|(\mathbf{r}) \exp(i\Phi). \quad \text{(B4)}$$

The total phase can be written in the form $\Phi = \Phi_L + \Phi_R + \Phi_{ns}$, where

$$\Phi_{L(R)}(\mathbf{r}) = \arctan\left(\frac{y - y_{R(L)}}{x - x_{R(L)}} \right)$$

are the vortex phases and $\Phi_{ns}(\mathbf{r})$ is a regular part of the phase. At the region $x < 0$, we can make the gauge transformation removing the phase $\Phi_R(\mathbf{r})$, since it does not contain singularities. After this transformation, we can assume that the fields $\mathbf{A}$, $\Delta_{1,2}$, and $f_{1,2}^{(+)}$ correspond to the solutions for a single vortex placed at the point $\mathbf{r_L}$ weakly perturbed by the presence of the second vortex

$$\mathbf{A} = \mathbf{A_v} + \delta\mathbf{Q}, \quad \Delta_j = \Delta_{vj} + \delta\Delta_j,$$

$$f_j = f_{vj} + \delta f_j, \quad f_j^+ = f_{vj}^+ + \delta f_j^+,$$

where we have introduced the superfluid velocity induced by the second vortex $\delta\mathbf{Q} = \mathbf{A_R} - \nabla\Phi_R$. Then, we obtain

$$\delta I_j = (\delta\Delta_j f_{vj}^+ + \delta\Delta_j^* f_{vj}) + (\Delta_{vj}\delta f_j^+ + \Delta_{vj}^* \delta f_j) + i v_{Fj}(g_{vj} - 1)\mathbf{n_p}\delta\mathbf{Q} + 2\tilde{\omega}_n \delta g_j + v_{Fj}\frac{\delta g_j}{2}\mathbf{n_p}\nabla(\ln f_{vj} - \ln f_{vj}^+) + v_{Fj}\frac{(g_{vj}-1)}{2}\mathbf{n_p}\nabla\left(\frac{\delta f_j}{f_{vj}} - \frac{\delta f_j^+}{f_{vj}^+}\right), \quad \text{(B5)}$$

where

$$\delta g_j = -(f_{vj}\delta f_j^+ + f_{vj}^+ \delta f_j)/2g_{vj}.$$

The last two terms in Eq. (B5) can be rewritten as

$$\frac{1}{2g_v}\left[\delta f(\mathbf{n_p}\nabla) f_v^+ - \delta f^+(\mathbf{n_p}\nabla) f_v\right], \quad \frac{(\mathbf{n_p}\nabla)}{2}\left[(g_v - 1)\left(\frac{\delta f}{f_v} - \frac{\delta f^+}{f_v^+}\right)\right]. \quad \text{(B6)}$$

The first term in this expression cancels with the second and fourth terms in Eq. (B5). For the variation of magnetic field energy in Eq. (B1), we obtain

$$\mathbf{H_v}\delta\mathbf{H} = \nabla\cdot(\delta\mathbf{Q}\times\mathbf{H_v}) + \nabla\times\mathbf{H_v}\cdot\delta\mathbf{Q}.$$

Then, we are left with the nonzero terms

$$\delta F = \nabla\cdot\delta\mathbf{Q}\times\mathbf{H_v} - \frac{T}{2\kappa^2}\sum_{j,\omega_n} n_j v_{Fj} \times \int_0^{2\pi} d\theta_p \nabla\cdot\mathbf{n_p}\left[(g_{vj}-1)\left(\frac{\delta f_j}{f_{vj}} - \frac{\delta f_j^+}{f_{vj}^+}\right)\right]. \quad \text{(B7)}$$

The energy of vortex interaction is $E_{\rm int} = 2\int \delta F d\mathbf{r}$. It can be expressed through the integral over the line $x = 0$ so that $E_{\rm int} = 2\int_{-\infty}^{\infty} dy\, \mathbf{x}\cdot\mathbf{e}_{\rm int}$:

$$\mathbf{e}_{\rm int} = \delta\mathbf{Q}\times\mathbf{H_v} - \frac{T}{2\kappa^2}\sum_{j,\omega_n} n_j v_{Fj} \times \int_0^{2\pi} d\theta_p \mathbf{n_p}\left[(g_{vj}-1)\left(\frac{\delta f_j}{f_{vj}} - \frac{\delta f_j^+}{f_{vj}^+}\right)\right]. \quad \text{(B8)}$$

To evaluate the second term in Eq. (B8), it is convenient to bring Eq. (1) to the gauge-invariant form[23] decomposing the gap functions into amplitude and phase (B4) and transforming the Green's functions as $f \to f e^{i\Phi}$, $f^+ \to f^+ e^{-i\Phi}$. Then, at the line $x = 0$, we can put

$$f_{vj} = f_{0j} + f_{Lj}, \quad f_{vj}^+ = f_{0j} + f_{Lj}^+,$$

where $f_{0j} = \Delta_{0j}/\sqrt{\Delta_{0j}^2 + \omega_n^2}$. Also, we denote $\delta f_j = f_{Rj}$, $\delta f_j^+ = f_{Rj}^+$ [L (R) stand for left (right) vortices]. Therefore, up to the second-order terms, we obtain

$$(g_{vj}-1)\left(\frac{\delta f_j}{f_{vj}} - \frac{\delta f_j^+}{f_{vj}^+}\right) = \frac{g_{0j}-1}{f_{0j}}(f_{Rj} - f_{Rj}^+) - \frac{1}{2g_{0j}}(f_{Lj} + f_{Lj}^+)(f_{Rj} - f_{Rj}^+) + \frac{g_{0j}-1}{f_{0j}^2}(f_{Rj}^+ f_{Lj}^+ - f_{Rj} f_{Lj}). \quad \text{(B9)}$$

Now we use the symmetry relations $f_{L,R}(n_x,n_y) = f_{R,L}^*(-n_x,n_y)$ and $f^*(-\mathbf{n_p}) = f^+(\mathbf{n_p})$. Then, the contribution to the interaction energy (B8) from the first-order term in

Eq. (B9) cancels with the analogous contribution from the left vortex. Also, from the symmetry relations, we obtain

$$\begin{aligned} \mathrm{Re}\int_0^{2\pi} \cos\theta_p f_L f_R d\theta_p = 0, \\ \mathrm{Re}\int_0^{2\pi} \cos\theta_p f_L^+ f_R^+ d\theta_p = 0. \end{aligned} \tag{B10}$$

On the other hand,

$$\mathrm{Im}\int_0^{2\pi} \cos\theta_p (f_L f_R - f_L^+ f_R^+) d\theta_p = 0.$$

Therefore, we get for the interaction energy

$$E_{\mathrm{int}} = 2\int_{-\infty}^{\infty} dy\, \tilde{E}_{\mathrm{int}}(y),$$

where

$$\tilde{E}_{\mathrm{int}} = H_v Q_v + T\sum_{j=1,2}\sigma_j \sum_{\omega_n>0}\frac{\Delta_{0j}}{4\omega_n} \times \int_0^{2\pi} d\theta_p \cos\theta_p (f_{Lj} f_{Rj}^+ - f_{Lj}^+ f_{Rj}), \tag{B11}$$

and $\sigma_j = \kappa^{-2} n_j v_{Fj}$.

[1] V. L. Ginzburg and L. D. Landau, Zh. Eksp. Teor. Fiz. **20**, 1064 (1950); L. D. Landau, *Collected Papers* (Oxford: Pergamon Press, 1965), p. 546.

[2] P. G. de Gennes, *Superconductivity of Metals and Alloys* (Addison-Wesley, New York, 1989).

[3] A. A. Abrikosov, Sov. Phys. JETP **5**, 1174 (1957) [Zh. Eksp. Teor. Fiz. **32**, 1442 (1957)].

[4] U. Klein, J. Low Temp. Phys. **69**, 1 (1987).

[5] A. E. Jacobs, J. Low Temp. Phys. **10**, 137 (1973).

[6] E. Babaev and M. Speight, Phys. Rev. B **72**, 180502 (2005).

[7] E. Babaev, A. Sudbø, and N. W. Ashcroft, Nature (London) **431**, 666 (2004).

[8] E. Babaev, Phys. Rev. Lett. **89**, 067001 (2002).

[9] V. Moshchalkov, M. Menghini, T. Nishio, Q. H. Chen, A. V. Silhanek, V. H. Dao, L. F. Chibotaru, N. D. Zhigadlo, and J. Karpinski, Phys. Rev. Lett. **102**, 117001 (2009).

[10] E. Babaev, J. Carlstrom, and M. Speight, Phys. Rev. Lett. **105**, 067003 (2010).

[11] J. Carlstrom, E. Babaev, and M. Speight, Phys. Rev. B **83**, 174509 (2011).

[12] J. Carlstrom, J. Garaud, and E. Babaev, e-print arXiv:1101.4599.

[13] H. Suhl, B. T. Matthias, and L. R. Walker, Phys. Rev. Lett. **3**, 552 (1959).

[14] T. Nishio, V. H. Dao, Q. Chen, L. F. Chibotaru, K. Kadowaki, and V. V. Moshchalkov, Phys. Rev. B **81**, 020506(R) (2010).

[15] A. Gurevich, Phys. C (Amsterdam) **456**, 160 (2007).

[16] K. Tanaka, M. Eschrig, and D. F. Agterberg, Phys. Rev. B **75**, 214512 (2007).

[17] M. C. Leung and A. E. Jacobs, J. Low Temp. Phys. **11**, 395 (1973).

[18] L. Kramer, Phys. Rev. B **3**, 3821 (1971).

[19] W. Pesch and L. Kramer, J. Low Temp. Phys. **15**, 367 (1973).

[20] G. Deutscher and P. G. de Gennes, in *Superconductivity*, edited by R. D. Parcs (Marcel Dekker, New York, 1969), Vol. 2, p. 1005.

[21] G. Eilenberger and H. Buttner, Z. Phys. **224**, 335 (1969).

[22] G. Eilenberger, Z. Phys. **214**, 195 (1968).

[23] T. Dahm, S. Graser, C. Iniotakis, and N. Schopohl, Phys. Rev. B **66**, 144515 (2002).